Structure and photocatalytic activity of maleic anhydride-functionalized TiO$_2$ nanoparticles by a simple method

Pável César Hernández Del Castillo[1*], Saúl Robles Manuel[2], Facundo Ruiz[2] and Vicente Rodríguez González[1]

Abstract

Titanium dioxide (TiO$_2$) nanoparticles were functionalized with maleic anhydride (MA). The extension of adsorbed MA on the TiO$_2$ was evaluated by ultrasonic and magnetic stirring. Total Organic Carbon and Thermogravimetric Analysis confirmed the presence of surface MA even after the washing process. The Fourier Transform Infrared and UV-Vis Diffuse Reflectance spectra clearly showed the chemical anchored maleic anhydride on the TiO$_2$ surface as bidentate bridging adsorption. The surface modification of TiO$_2$ extended its light absorption range to the visible light region reducing its bandgap energy from 3.05 to 2.55 eV. X-Ray Diffraction patterns showed that the TiO$_2$ functionalized presented a mixture of anatase and rutile phases without any crystalline phase transformation after MA chemisorption process. The functionalization percentage and the reaction efficiency for the TiO$_2$ with 5 wt% MA sample were 3.6 and 69%, respectively, as shown by Differential Thermal Analysis and Thermogravimetric Analysis. The performance of pure and functionalized TiO$_2$ samples were evaluated in the photocatalytic degradation of the Methyl Orange dye under ultraviolet light. TiO$_2$ with 5 wt% MA produced a maximum degradation of 97% after 90 min, 3% higher than the commercial TiO$_2$.

Keywords: Functionalization, Titanium dioxide nanoparticles, Photocatalysis, Maleic anhydride, Nanostructures

1 Introduction

The study of metal oxides has been of great interest in developing hybrid materials, catalysis, and solar cells. For example, titanium dioxide (TiO$_2$) is the most popular photocatalyst because of its excellent physical and chemical characteristics. However, it only absorbs 4% of sunlight [1]. The light absorption range of TiO$_2$ can be shifted to the visible region by modifying its structure or surface. There are some methods to improve the physical and chemical properties of TiO$_2$, such as etching, photo-deposition of metals, organic compounds anchoring, and metal ions doping [2–5].

Previous studies have been focused on increasing the ability of TiO$_2$ to capture photons outside the ultraviolet

(UV) light absorption range [6, 7]. Chen et al. [8] investigated the photocatalytic activity of Fe$_2$O$_3$/TiO$_2$ functionalized biochar in Fenton processes; the percentages degradation of Methyl Blue, Rhodamine B, and Methyl Orange (MO), were 78, 67, and 83%, respectively. Chalasani and Vasudevan [9] observed that even after 10 cycles, the efficiency of the Fe$_3$O$_4$@TiO$_2$ functionalized with carboxymethyl-β-cyclodextrin for the photocatalytic degradation of Bisphenol A remains at high level, maintaining 90% efficiency as compared to the first use efficiency. Also, Sun et al. [10] reported the surface modification of TiO$_2$ with polydopamine in the removal of Rhodamine B, showing a percentage degradation of 99% under UV light radiation. In addition, Galoppini [11] considered it necessary to know the physicochemical properties of the solid surfaces to obtain a good stability between the organic and inorganic phases.

* Correspondence: pavel.hernandez@ipicyt.edu.mx
[1]Advanced Materials Department, The Institute for Scientific and Technological of San Luis Potosi, 78216 San Luis Potosi, Mexico
Full list of author information is available at the end of the article

Commonly, the maleic anhydride (MA) has been used as a coupling agent in the functionalization of nanoparticles because it serves as a "seed molecule" capable of anchoring organic compounds [12–14]. However, there are a few investigations about surface modification of metal oxides with MA. This compound has two functional groups: carboxyls and alkenes. The carboxyl group interacts chemically on the TiO_2 surface. The sensitization of inorganic nanoparticles surface with MA induces the transfer of electrons from the bonds of the organic compound to the conduction band of TiO_2 by photonic excitation. The visible light absorption in the solid is increased when the amount of anchored carboxylate groups is higher. This condition gives it the ability to have more photon receptor sites [15, 16]. The decomposition of MA on the surfaces (1 0 1), (1 0 0), and (0 0 1) of TiO_2 single crystal (anatase) indicates the presence of two types of oxygen on the plane (0 0 1), which are found by X-ray photoelectron spectroscopy. This observation explains the bidentate adsorption geometry formed by a ring-opening reaction of MA on the planes (1 0 1) and (0 0 1). Also, four oxygen equivalents on the TiO_2 surface indicate a similar behavior of MA for carboxylic acid [12]. Wilson et al. [14] found similar results about the adsorption of MA on the plane (0 0 1) of single rutile crystals. Dissociative adsorption was suggested to be the most stable configuration of the TiO_2/MA system. The MA is adsorbed by the Ti_{5C}^{4+} species on the TiO_2 surface, interacting with the oxygen atoms [17–20]. Others have mentioned the procedures to anchor MA on the solids [21–23]; however, such procedures imply using highly specialized methodologies such as ultra-high vacuum systems. Therefore, this work develops an easy and efficient method of functionalizing TiO_2 nanoparticles with MA.

2 Materials and methods

2.1 Materials

The MA ($C_4H_2O_3$, MW = 98.06 g mol^{-1}, ≥ 99.0% pure) was supplied by Sigma-Aldrich. The solvents used as reaction media, toluene (TO) and ethanol (ET), were purchased from CTR Scientific. TiO_2 nanoparticles were purchased from Degussa P-25 with a mean particle size of ~21 nm, a surface area of 50 m^2 g^{-1}, and a mixture of anatase (~80%) and rutile (~20%). The dye used in the photocatalytic tests was MO ($C_{14}H_{14}N_3NaO_3S$, MW = 327.3 g mol^{-1}) from Sigma-Aldrich.

2.2 Synthesis of functionalized TiO_2

0.3 g of TiO_2 were dispersed in 190 mL of ET or TO. The mixture was stirred and heated to 50 or 80 °C depending on the solvent used. Then, MA was dissolved in 10 mL of solvent while adding slowly. After that, the reaction was brought to a temperature below the boiling points for ET at 70 °C, TO at 105 °C. It was maintained at constant reflux for 4.5 h. Finally, the solvent was separated by centrifugation and decanting to recover the functionalized nanoparticles. The TiO_2 nanoparticles were prepared with different concentrations of MA: 2 wt% (1TiMA) and 5 wt% (2TiMA).

2.3 Washing methodology

Functionalized TiO_2 nanoparticles were washed using 500 mL of deionized water. First, 100 mL were used to wash under ultrasonic stirring for 30 min. Next, 400 mL were used to wash by magnetic stirring for 240 min. Finally, the nanoparticles were filtered and dried at 120 °C to get the powered functionalized materials.

2.4 Synthesis of modified TiO_2 by physical methods

A comparative study with other two synthesis approaches was carried out to determine the effectiveness of the functionalization method. The first method, known as a physical mixture, consisted of a simple combination of MA with TiO_2 powders at room temperature. The second one, the impregnation method, was done under similar conditions as in the functionalization method but at room temperature to get dried powered materials.

2.5 Quantification of chemically adsorbed MA on the TiO_2 surface

The initial weights of MA in the synthesis of the samples 1TiMA-ET and 2TiMA-ET were 0.0061 and 0.0158 g, respectively. At the end of the reaction and the post-functionalization treatments (washing and drying), the final weights of MA obtained by Thermogravimetric Analysis (TGA) were 0.0046 and 0.0108 g. From this data, the actual amount of chemically adsorbed MA on the TiO_2 surface can be quantified.

2.6 Photocatalytic procedure

A kinetic study evaluated the photocatalytic activity of the functionalized samples to degrade the dye under UV radiation using 40 mg of catalyst and 40 mL of MO solution (4×10^{-5} M), maintaining room temperature using a cooling system. Adsorption tests were performed on the catalysts in a MO solution using magnetic stirring without UV light for 60 minutes. After that, the solution was irradiated by 4 UV lamps Vilber-Lourmat T-15L (15 W, λ = 365 nm) for 90 min, and its absorbance was analyzed every 10 min by UV-Vis. Previously, the solid-liquid phases were separated by centrifugation.

2.7 Characterization of the samples

The thermal behavior of the modified TiO_2 was determined by TGA and Differential Thermal Analysis (DTA) on an SDT Q600 of TA. The heating rate was 10 °C

min^{-1} from 25 to 600 °C. The Fourier Transform Infrared (FTIR) spectra were recorded using a Nicolet 670 spectrometer from 400 to 4000 cm^{-1}. The samples were mixed with spectroscopic grade KBr, measured with 32 scans with a resolution of 4 cm^{-1}. Diffuse Reflectance Spectra (DRS) were collected by S2000 UV-Vis spectrophotometer from Ocean Optics using Ca_2SO_4 as a blank. The crystal structure of the samples was determined by X-Ray Diffraction (XRD, GBC-Difftech MMA model) using Cu Kα irradiation at λ = 1.54 A° in a range from 10 to 80° of 2θ, a speed recording of 2° min^{-1} and an interval of 0.02°. The absorption spectra of the MO were obtained by S2000 UV-Vis spectrophotometer using an integration time of 100 ms and 5 scans. In addition, the residual water used in the washings was analyzed by Total Organic Carbon (TOC, VCPH-CPN, Shimadzu) to determine the TOC concentration.

3 Results and discussion

3.1 Chemical stability
The physical adsorption between the organic compounds and the TiO_2 surface has a lower cohesion than the chemical adsorption. Therefore, these attraction forces can be eliminated by washing with ultrasonic and magnetic stirring. These processes removed the unreacted MA from the functionalized TiO_2 surface because of its high solubility in water. The washing effectiveness was confirmed by the decrease in the TOC concentration of the wastewater collected after washings. Figure 1 shows the progressive decrease of the TOC concentration when the volume of water is increased. The concentrations of the last three washes were lowest and very similar, which confirms the loss of organic material. As a result, the minimum volume of water
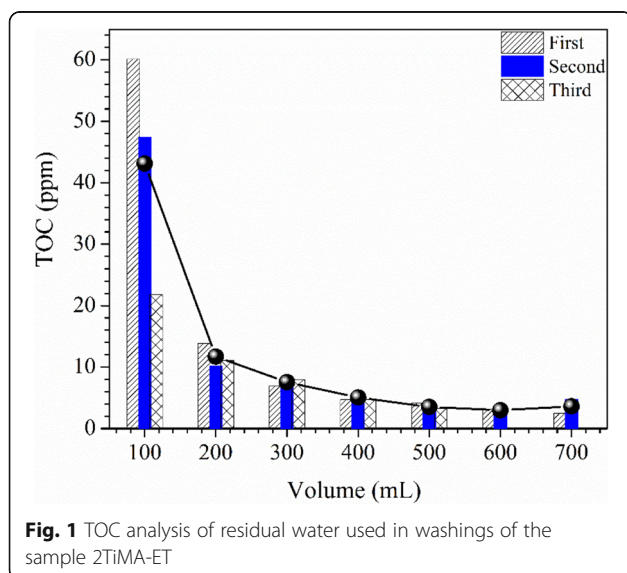
required for the total desorption of unreacted MA and residual solvent was 500 mL.

TGA curves show a noticeable decrease in the percentage of weight loss of the washed samples in the temperature range from 200 to 600 °C, due to the decomposition and desorption of chemically adsorbed MA on the TiO_2 surface shown in Fig. 2. In addition, sample 2TiMA-ET had a more significant weight loss than sample 1TiMA-ET due to the increased anchored MA on the TiO_2 surface. This observation showed the outstanding contribution of washings in eliminating physically adsorbed organic compounds from the functionalized TiO_2 surface. Before the characterization, these trials were very important to perform the exclusive quantification of chemically adsorbed MA on the TiO_2 surface.

3.2 Crystal structure
The XRD patterns were indexed with the crystallographic planes corresponding for each phase according to the JCPDS 21-1272 (anatase) and JCPDS 03-1122 (rutile) cards. Figure 3 shows the XRD patterns of the surface-modified TiO_2 samples by physical mixture, impregnation, and functionalization methods. All the patterns, corresponding to the pristine sample and the modified samples, showed similar crystalline phases (anatase and rutile), indicating that the surface MA functionalization of the TiO_2 has no effect in its crystalline structure. However, there is a slight shift to the left in the diffraction pattern of the sample 2TiMA-ET synthesized by functionalization (chemical method). While the XRD patterns obtained of the samples synthesized by physical mixture and impregnation methods did not show any shift because its surface modification is by simple physical interaction. The shift in the diffraction angle is observed due to the transparency effect


Fig. 1 TOC analysis of residual water used in washings of the sample 2TiMA-ET

Fig. 2 TGA curves of the functionalized samples before and after washing process
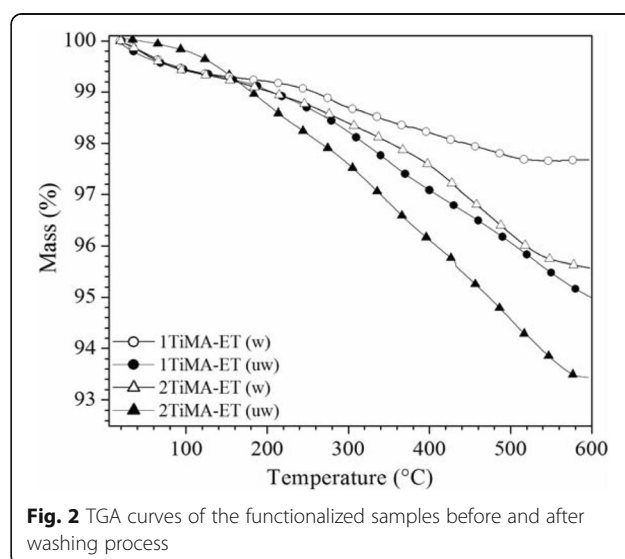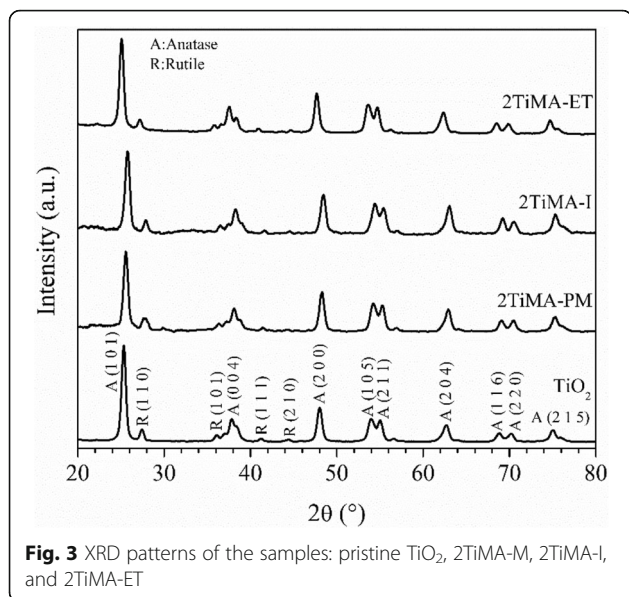
Fig. 3 XRD patterns of the samples: pristine TiO_2, 2TiMA-M, 2TiMA-I, and 2TiMA-ET

presented when the X-ray beam interacts with the chemically anchored MA on the TiO_2 surface [24].

3.3 FTIR spectroscopy

Fig. 4 shows the FTIR spectra of the functionalized samples 1TiMA-ET and 2TiMA-ET, previously washed and dried. The asymmetric (1869 cm^{-1}) and symmetric (1783 cm^{-1}) C=O vibrations of the MA molecule were not observed. However, two bands at 1714 cm^{-1} and another at 1696 cm^{-1} were found on the band centered at 1700 cm^{-1}. The band centered at 1570 cm^{-1} of the spectrum of the sample 2TiMA-TO is composed of COO$^-$ symmetric vibrations and stretching vibrations of the C=C bond.

These assumptions were confirmed by deconvolutions of the FTIR spectra, as shown in Fig. 5. The fit was done in two and three components using Lorentzian functions
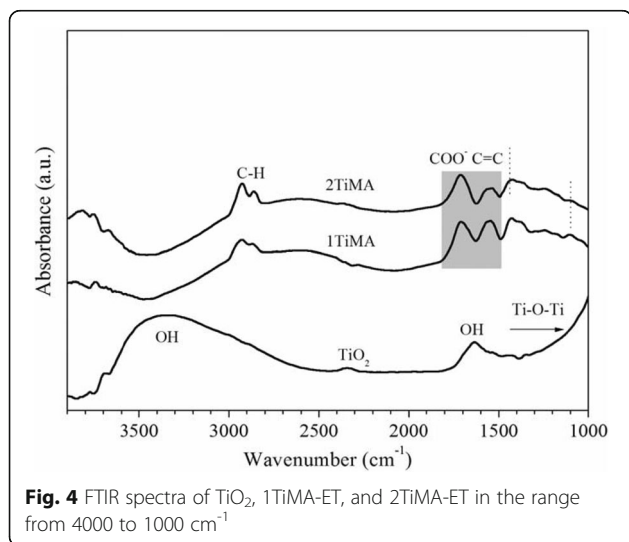

Fig. 4 FTIR spectra of TiO_2, 1TiMA-ET, and 2TiMA-ET in the range from 4000 to 1000 cm^{-1}

according to a similar procedure for an XPS spectrum [25, 26]. The most precise fit presented for the band centered at 1700 cm^{-1} resulted in two components. The deconvolution showed two peaks around 1714 and 1696 cm^{-1} which were considered asymmetric vibrations of COO$^-$. The band centered at 1570 cm^{-1} was fitted into three components. The deconvolution revealed the contribution of three different bands. Two at 1546 and 1514 cm^{-1} are assigned to different symmetric vibrations of COO$^-$, and the last one at 1584 cm^{-1} corresponding to the stretching vibration of C=C, which has a shift of 10 cm^{-1} compared with the absorption band on the FTIR spectra of the pure MA [27–29]. Mirone and Chiorboli [27] observed a similar absorption band at 1587 cm^{-1}, when the maleic acid was used. This slight shift is justified because there is no direct interaction between the C=C bond and the solid surface. Vibration bands of C-O were observed at 1160 and 1096 cm^{-1}. Another well-defined band at 1220 cm^{-1} was assigned to a bending vibration in the plane of the C-H bond [28, 29].

The difference between the asymmetric and the symmetric stretch vibrations of the carboxylic acids ($\Delta\gamma_{as-s}$) defines the adsorption geometry of the MA molecule on the solid surface. Commonly, the ranges for monodentate adsorption are 350-500 cm^{-1}, bidentate bridging are 150-180, and 60-100 cm^{-1} for bidentate chelating. In our case, there is a $\Delta\gamma_{as-s}$ of 150 cm^{-1}, approximately. Therefore, the adsorption form of the MA on the TiO_2 surface corresponds to bidentate bridging, as shown in Fig. 6C. Furthermore, the vibration band at 1160 cm^{-1} assigned to the C-O bond supports the assumption of bidentate bridging adsorption. Others authors observed a stretching vibration of the C-O bond near 1140 cm^{-1} [30, 31], which confirms the bidentate geometry of the propoxy species on the TiO_2 surface.

The TiO_2 nanoparticles used in our study consist mainly of anatase. The (1 0 1) plane is the most common surface for this phase. Therefore, it favors the bidentate bridging adsorption, which involves the ring-opening of the MA molecule [32, 33]. Kim and Barteau [34] observed an identical behavior in the carboxylic acids and other analogous organic molecules.

3.4 TG and DT analyses

The thermal behavior of the sample 2TiMA-ET had two main weight losses, as shown in Fig. 7. The first one was about 1.2% in a temperature range from 25 to 200 °C, attributed to the elimination of water, residual solvent, and possible remnants of unreacted MA [35]. Feist et al. [36] observed the same endothermic peak as the typical behavior of a desorption process. The second weight loss was 4.1%, which coincided with a strong exothermal effect in the range from 200 to 580 °C on the thermal curve, attributed to the decomposition and desorption of anchored MA. Nikumbh et al. [35] observed exothermic
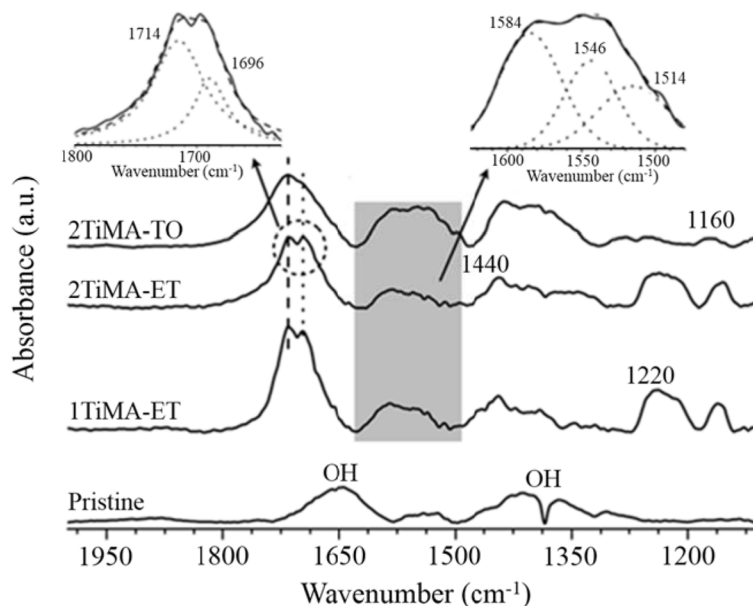
Fig. 5 FTIR spectra of TiO$_2$, 1TiMA-ET, 2TiMA-ET, and 2TiMA-TO in the range from 2000 to 1100 cm^{-1}

peaks related to the decomposition of maleates compounds between 250 and 450 °C. Decomposition-desorption of MA on the TiO$_2$ mainly occurred between 280 and 470 °C. Desorption of carbonates due to the decomposition of MA was observed at 470 °C, the desorption of acetylene and CO$_2$ occurred at 500 °C [5, 21].

The functionalization degree and the reaction efficiency of the samples 1TiMA-ET and 2TiMA-ET (as shown in Table 1) were calculated from the experimental conditions of the reaction and TGA results, using the Eqs. (1) and (2):

$$
\text{Functionalization degree (\%)} = \left(\frac{\text{anchored MA (g)}}{\text{TiO}_2 \text{ used (g)}} \right) \times 100 \tag{1}
$$

$$
\text{Reaction efficiency (\%)} = \left(\frac{\text{Experimental result}}{\text{Theoretical result}} \right) \times 100
$$

The functionalization process suggests there is a low concentration of anchored MA molecules on the TiO$_2$ surface due to steric hindrance when occupying surface
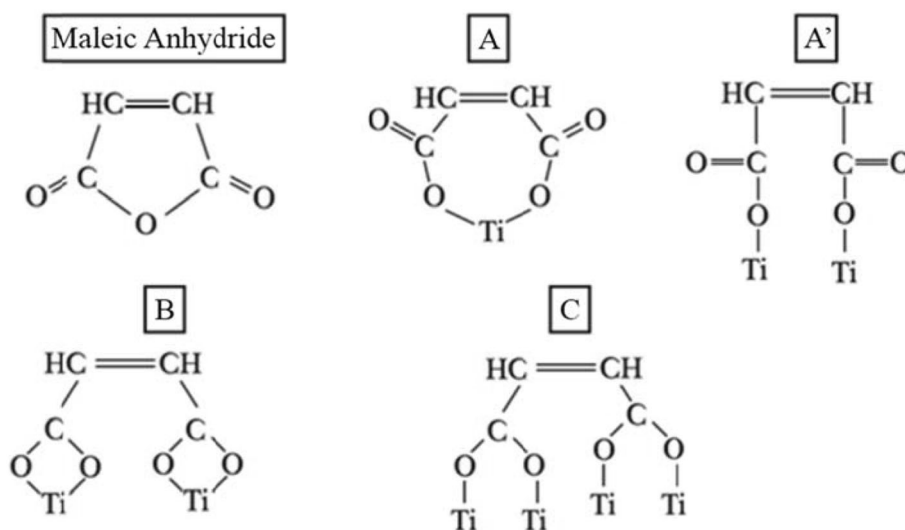

Fig. 6 Possible adsorption modes of the MA molecule on the TiO$_2$ surface: A and A') monodentate, B) bidentate chelating, and C) bidentate bridging

Fig. 7 TG-DTA curves of the sample 2TiMA-ET from 25 to 600 °C

Fig. 8 UV-Vis diffuse reflectance spectra of the samples: pristine TiO_2, 2TiMA-M, 2TiMA-I, 2TiMA-TO, and 2TiMA-ET
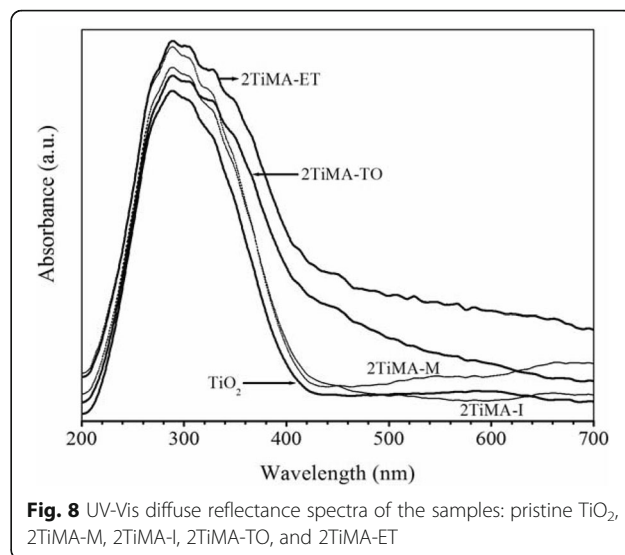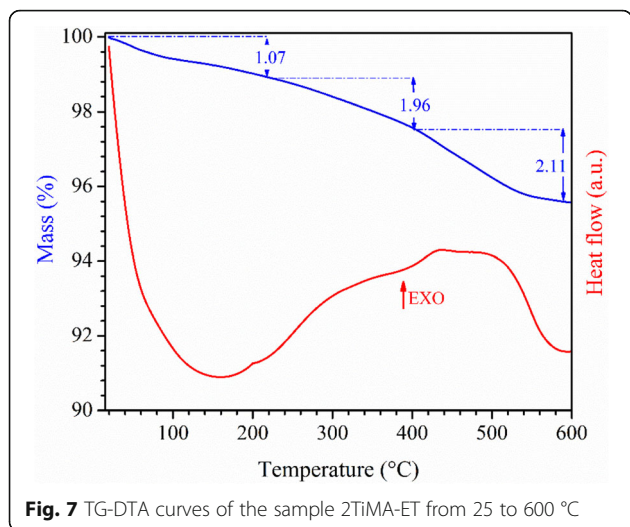
area in the TiO_2 nanoparticles. Therefore, the TiO_2 surface is partially functionalized and has a limited amount of anchored reactant on all the reaction sites located on the TiO_2 surface. As a result, a decrease in the reaction efficiency of the sample 2TiMA-ET for the sample 1TiMA-ET was observed.

3.5 UV-Vis DRS

The UV-Vis spectra of modified TiO_2 samples synthesized by physical and chemical methods are shown in Fig. 8. The functionalized samples exhibited a noticeable increase in visible light absorption and decreased bandgap energy. For example, the area under the curve of the 2TiMA-ET absorption spectrum, integrated from 400 to 700 nm, increased 36 units^2 compared with that of pristine TiO_2. On the other hand, the samples performed by physical methods did not show any increase in the visible light region concerning pristine TiO_2. This observation confirms the presence of anchored MA on the TiO_2 surface and means that it can be excited with less energy, thus extending its absorption range from UV light to the visible region. Also, functionalized samples were able to absorb visible light beyond 400 nm. However, the MA only absorbs at 204 nm corresponding to the UV region. Therefore, the visible light absorption observed in the UV-Vis spectra of the functionalized samples is attributed to the physical obstacle presented when the

light penetrates through molecular chains of anchored MA to interact with the TiO_2 surface.

Figure 9 shows a decrease in the bandgap energy of TiO_2 from 3.05 to 2.55 eV that extended to visible region for the functionalized sample 2TiMA-ET due to the anchored MA on the TiO_2 surface. The samples 2TiMA-ET and 2TiMA-TO synthesized by the chemical method showed a significant decrease in its bandgap energy compared with the samples 2TiMA-physical mixture and 2TiMA-impregnation method obtained by physical methods, which showed similar behavior in the visible light absorption to commercial TiO_2. The bandgap energy values of the functionalized samples were similar to the results of other authors with the dye-sensitized TiO_2 surface because the dye can absorb visible light [37]. However, our synthesis method is simpler

Table 1 Functionalization degree and reaction efficiency of the samples 1TiMA-ET and 2TiMA-ET

Sample	w_i[a] (g)	w_f[b] (g)	FD (%)	Reaction efficiency (%)
1TiMA-ET	0.0061	0.0046	1.54	76
2TiMA-ET	0.0158	0.0108	3.61	69

[a] Initial weight of MA in the reaction
[b] Final weight of anchored MA on the TiO_2 surface obtained by DTA

Fig. 9 DRS spectra and bandgap energy of the samples: pristine TiO_2, 2TiMA-M, 2TiMA-I, 2TiMA-ET, and 2TiMA-TO
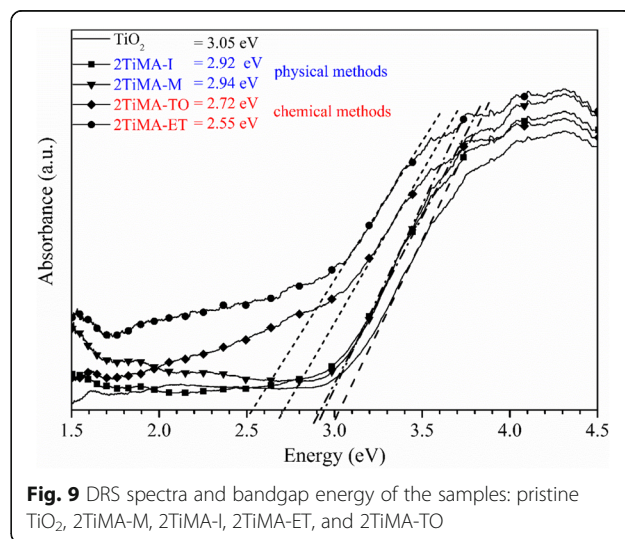
and cheaper than the other functionalization processes with complex and expensive methods [38, 39].

3.6 Photocatalytic tests

The photocatalytic analysis was carried out by degrading MO under UV light radiation using pristine TiO_2 and 2TiMA-ET as photocatalysts, as shown in Fig. 10. All the UV-Vis spectra exhibit a decrease in the absorbance of the band centered at 463 nm (absorption wavelength attributed to -N=N- bond) due to the progressive degradation of the MO solution. The catalysts were tested using the same conditions to determine their capacity to adsorb dye without light. When the commercial TiO_2 is functionalized with MA, its surface adsorption is increased. However, thus physical ability is not significant because the low percentage of anchored MA cannot adsorb much dye. For the kinetic study, the photodegradation evaluation only is considered after the adsorption tests. The UV-Vis absorbance spectra obtained to degrade the MO solution using the functionalized sample 2TiMA-ET (Fig. 10b), and the commercial TiO_2 (Fig. 10a) showed a progressive decrease of the absorption band of the MO due to its degradation. The MO solution was degraded using both catalysts after 90 min of reaction time based on the absorbance curves.
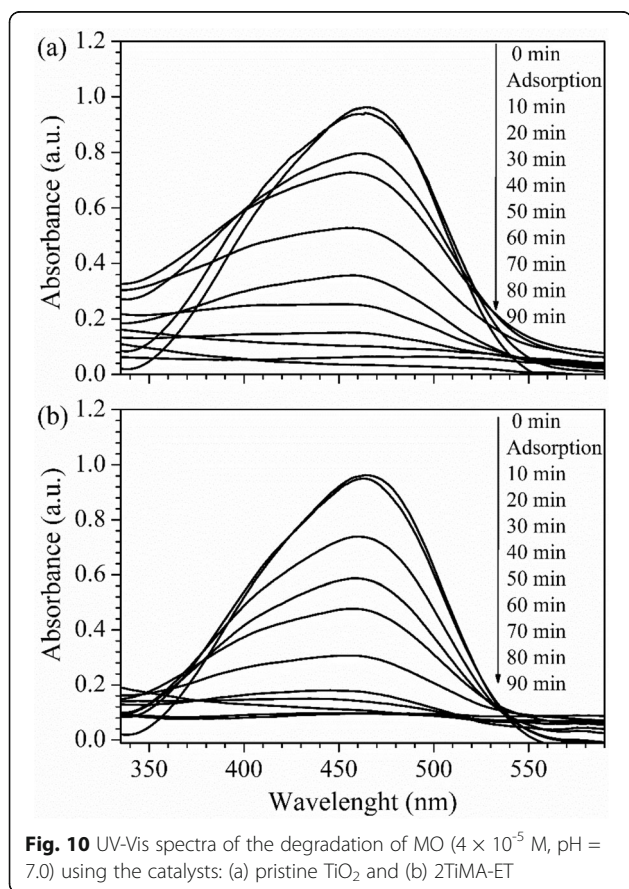
However, there is a faster degradation rate of the MO solution using the functionalized TiO_2. The surface modification with MA inhibits the recombination of the hollow-electron pair and decreases the bandgap to 2.55 eV; this characteristic facilitates a more significant transfer of electrons and improves photocatalytic activity. Based on experimental studies, a schematic diagram of the band levels of the 2TiMA-ET composite and the possible mechanism of the photocatalytic reaction in the MO dye degradation are proposed and illustrated in Fig. 11.

The commercial and functionalized TiO_2 were photocatalytically evaluated by kinetic parameters calculated from the MO degradation with UV light. These parameters were the reaction's constant rate, conversion, and half-life, as shown in Table 2. The conversion reaction of functionalized TiO_2 was improved by 3.2% compared with the commercial TiO_2, as shown in Fig. 12. The reaction order is first according to the Langmuir-Hinshelwood model due to its high linear correlation of values. The rate constant can be obtained through the equation $lnc = -kt + lnc0$ by linear regression, where (k) is the rate constant, (c) is concentration, and (t) is the reaction time. One of the limitations to obtain a higher reaction rate is a high initial dye concentration because it can hinder the free passage of photons in the solution to be degraded [38, 39]. The constant rate and half-life of reaction also showed better results with the functionalized sample 2TiMA-ET than for the pristine TiO_2. This result was expected because of the synergy produced between the organic molecules and the TiO_2 surface. These conditions favor the production of a greater amount of electron acceptor sites that retard the recombination of the electron-hole pair and the presence of oxidizing agents on the surface of TiO_2 nanoparticles [40]. Figure 13 shows the reuse tests for the TiO_2 and

**Fig. 10** UV-Vis spectra of the degradation of MO (4×10^{-5} M, pH = 7.0) using the catalysts: (a) pristine TiO_2 and (b) 2TiMA-ET

Fig. 11 Schematic diagram of the band levels of 2TiMA-ET and the possible reaction mechanism of the photocatalytic procedure
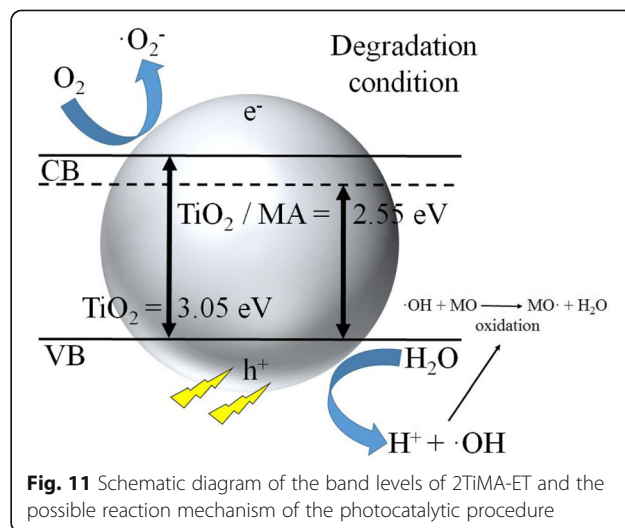
Table 2 Kinetic results of the photocatalytic degradation of MO (4×10^{-5} M) under UV radiation

Sample	k^a (min^{-1})	$C/C_0{}^b$	Conversion reaction (%)	$t_{1/2}{}^c$ (min)
TiO$_2$	0.032	0.058	94	22
2TiMA-ET	0.044	0.026	97	15.9

[a]Reaction rate
[b]Fraction of conversion reaction
[c]Half time of reaction

2TiMA-ET samples and found that the final degradation percentage of the MO dye (after 90 min) was reduced only by 7% after using the 2TiMA-ET for 4 consecutive times while for the commercial TiO$_2$ when is reused 4 times, the degradation efficiency is reduced by 13%. Thus, the 2TiMA-ET is the most stable and presents a higher photocatalytic activity in the degradation of MO than the commercial TiO$_2$. This work presented a greater efficiency in the photocatalytic degradation of the MO dye under UV light radiation (97% at 90 min using 2TiMA-ET) compared to other similar investigations where MO and other types of dyes were degraded [8–10].

4 Conclusions

The MA was chemically adsorbed onto the surface of the TiO$_2$ nanoparticles showing good stability after several washings. MA functionalization was confirmed by FTIR, DRS, and XRD results. The FTIR analysis showed vibration bands of bonds that indicate the chemical interaction between the MA molecules and the TiO$_2$ nanoparticles. The adsorption geometry of MA on the TiO$_2$ surface was determined as bidentate bridging. TG-DTA quantified the chemically adsorbed MA onto the TiO$_2$ nanoparticles. The reaction efficiencies of the
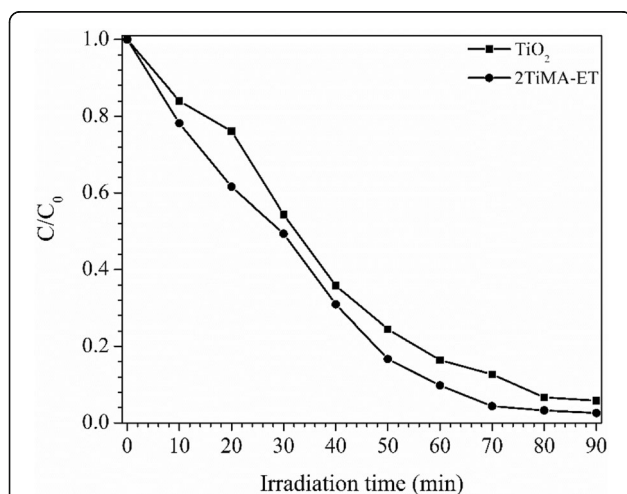
Fig. 12 The kinetics of MO (4×10^{-5} M, pH = 7.0) photo-degradation using the catalysts: pristine TiO$_2$ and 2TiMA-ET
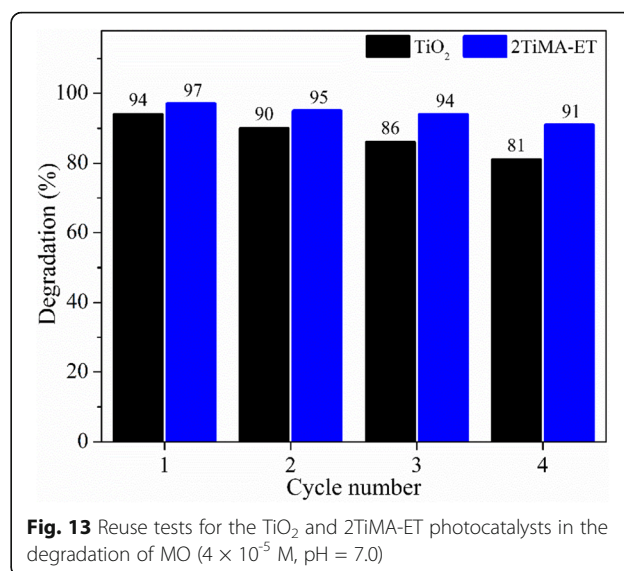
Fig. 13 Reuse tests for the TiO$_2$ and 2TiMA-ET photocatalysts in the degradation of MO (4×10^{-5} M, pH = 7.0)

samples 1TiMA-ET and 2TiMA-ET were 76 and 69%, respectively. The diffraction pattern of the functionalized sample 2TiMA-ET did not change its crystalline phases from the pristine TiO$_2$. However, the bandgap energy of TiO$_2$ decreased from 3.05 to 2.55 eV when its surface was functionalized with MA. DRS spectra show that the absorbance of the 2TiMA-ET sample was higher and more extended in the visible range of 400-800 nm than that for the TiO$_2$ pristine due to the presence of oxygen vacancy defects, which act as electron trapping centers and delay the electron-hole recombination. This higher absorbance is suitable because it increases the probability of photogeneration of electron-hole pairs, which are responsible for the generation of oxidizing agents that degrade the MO. As a result, the functionalized TiO$_2$ showed improvements in its photocatalytic properties, increasing 3.2% in the MO degradation rate compared with the commercial TiO$_2$.

Authors' contributions
Pável César Hernández-Del Castillo* carried out the experiments, discussed the results, and wrote the submitted manuscript; Saúl Robles-Manuel contributed to the discussion of results, supported ideas for the project, and helped to supervise trials. Facundo Ruiz contributed to the submitted version of the manuscript, provided critical feedback, and supervised the project's performance. Finally, Vicente Rodríguez-González contributed to the preparation and characterization of the samples and helped shape the research and the elaboration of the final manuscript. All authors read and approved the final manuscript.

Availability of data and materials

All data generated or analyzed during this study are fully available to give certainty to the work carried out.

Declarations

Competing interests

The authors declare that they have no known competing financial interests or personal relationships that could have influenced the work reported in this paper.

Author details

[1]Advanced Materials Department, The Institute for Scientific and Technological of San Luis Potosi, 78216 San Luis Potosi, Mexico. [2]Faculty of Sciences, Autonomous University of San Luis Potosi, 78290 San Luis Potosi, Mexico.

References

1. Sabry RS, Al-Haidarie YK, Kudhier MA. Synthesis and photocatalytic activity of TiO$_2$ nanoparticles prepared by sol-gel method. J Sol-Gel Sci Tech 2016;78:299–306.
2. Lucarelli L, Nadtochenko V, Kiwi J. Environmental photochemistry: quantitative adsorption and FTIR studies during the TiO$_2$-photocatalyzed degradation of Orange II. Langmuir 2000;16:1102–8.
3. Anpo M, Dohshi S, Kitano M, Hu Y, Takeuchi M, Matsuoka M. The preparation and characterization of highly efficient titanium oxide-based photofunctional materials. Annu Rev Mater Res 2005;35:1–27.
4. Rodriguez-Gonzalez V, Zanella R, del Angel G, Gomez R. MTBE visible-light photocatalytic decomposition over Au/TiO$_2$ and Au/TiO$_2$-Al$_2$O$_3$ sol-gel prepared catalysts. J Mol Catal A-Chem 2008;281:93–8.
5. Ren FJ, Ling YH, Feng JY. The role of W doping in response of hydrogen sensors based on MAO titania films. Appl Surf Sci 2010;256:3735–9.
6. Chen DH, Huang FZ, Cheng YB, Caruso RA. Mesoporous anatase TiO$_2$ beads with high surface areas and controllable pore sizes: a superior candidate for high-performance dye-sensitized solar cells. Adv Mater 2009;21:2206–10.
7. Takai A, Kamat PV. Capture, store, and discharge. Shuttling photogenerated electron across TiO$_2$-silver interface. ACS Nano 2011;5:7369–76.
8. Chen XL, Li F, Chen HY, Wang HJ, Li GG. Fe$_2$O$_3$/TiO$_2$ functionalized biochar as a heterogeneous catalyst for dyes degradation in water under Fenton processes. J Environ Chem Eng 2020;8:103905.
9. Chalasani R, Vasudevan S. Cyclodextrin-functionalized Fe$_3$O$_4$@TiO$_2$: reusable, magnetic nanoparticles for photocatalytic degradation of endocrine-disrupting chemicals in water supplies. ACS Nano 2013;7:4093–104.
10. Sun XT, Yan LT, Xu RX, Xu MY, Zhu YY. Surface modification of TiO$_2$ with polydopamine and its effect on photocatalytic degradation mechanism. Colloid Surface A 2019;570:199–209.
11. Galoppini E. Linkers for anchoring sensitizers to semiconductor nanoparticles. Coordin Chem Rev 2004;248:1283–97.
12. Lopez A, Bitzer T, Heller T, Richardson NV. Adsorption of maleic anhydride on Si (1 0 0)-2x1. Surf Sci 2001;477:219–26.
13. Bishop LM, Yeager JC, Chen X, Wheeler JN, Torelli MD, Benson MC, et al. A citric acid-derived ligand for modular functionalization of metal oxide surfaces via "click" chemistry. Langmuir 2012;28:1322–9.
14. Wilson JN, Titheridge DJ, Kieu L, Idriss H. Reactions of maleic anhydride over TiO$_2$ (0 0 1) single crystal surfaces. J Vac Sci Technol A 2000;18:1887–92.
15. Choi SK, Yang HS, Kim JH, Park H. Organic dye-sensitized TiO$_2$ as a versatile photocatalyst for solar hydrogen and environmental remediation. Appl Catal B-Environ 2012;121–2:206–13.
16. Zarzuela R, Moreno-Garrido I, Almoraima Gil ML, Mosquera MJ. Effects of surface functionalization with alkylalkoxysilanes on the structure, visible light photoactivity and biocidal performance of Ag-TiO$_2$ nanoparticles. Powder Technol 2021;383:381–95.
17. Bates SP, Kresse G, Gillan MJ. The adsorption and dissociation of ROH molecules on TiO$_2$ (110). Surf Sci 1998;409:336–49.
18. Zeng W, Liu TM, Wang ZC, Tsukimoto S, Saito M, Ikuhara Y. Oxygen adsorption on anatase TiO$_2$ (101) and (001) surfaces from first principles. Mater Trans 2010;51:171–5.
19. Kavathekar RS, Dev P, English NJ, MacElroy JMD. Molecular dynamics study of water in contact with the TiO$_2$ rutile-110, 100, 101, 001 and anatase-101, 001 surface. Mol Phys 2011;109:1649–56.
20. Cai YQ, Bai ZQ, Chintalapati S, Zeng QF, Feng YP. Transition metal atoms pathways on rutile TiO$_2$ (110) surface: distribution of Ti^{3+} states and evidence of enhanced peripheral charge accumulation. J Chem Phys 2013;138:154711.
21. Girol SG, Strunskus T, Muhler M, Woll C. Reactivity of ZnO surfaces toward maleic anhydride. J Phys Chem B 2004;108:13736–45.
22. Wilson JN, Idriss H. Reactions of glutaric acid on the TiO$_2$ (001) single crystal. Effect of surface reduction on the reaction pathway. Langmuir 2005;21:8263–9.
23. Gao YK, Traeger F, Shekhah O, Idriss H, Wöll C. Probing the interaction of the amino acid alanine with the surface of ZnO(1 0 $\overline{1}$ 0). J Colloid Interf Sci. 2009;338:16–21.
24. Kulg HP, Alexander LE. X-ray diffraction procedures: for polycrystalline and amorphous materials. 2nd ed. New York: Wiley; 1974.
25. Sprenger D, Anderson O. Deconvolution of XPS spectra. Fresen J Anal Chem 1991;341:116–20.
26. Ni J, Meunier FC, Robles-Manuel S, Barrault J, Valange S. Characterization of surface acidity of carbonated materials by IR-sensitive molecular probes: advantages of using tert-butyl cyanide. J Phys Chem C 2011;115:24931–6.
27. Mirone P, Chiorboli P. Infrared and Raman spectra and vibrational assignment of maleic anhydride. Spectrochim Acta 1962;18:1425–32.
28. Parker SF, Wilson CC, Tomkinson J, Keen DA, Shankland K, Ramirez-Cuesta AJ, et al. Structure and dynamics of maleic anhydride. J Phys Chem A 2001;105:3064–70.
29. Vogt N, Demaison J, Rudolph HD. Equilibrium structure and spectroscopic constants of maleic anhydride. Struct Chem 2011;22:337–43.
30. Nijhuis TAR, Visser T, Weckhuysen BM. The role of gold in gold-titania epoxidation catalysts. Angew Chem Int Edit 2005;44:1115–8.
31. Ruiz A, Van der Linden B, Makkee M, Mul G. Acrylate and propoxy-groups: contributors to deactivation of Au/TiO$_2$ in the epoxidation of propene. J Catal 2009;266:286–90.
32. Fang WQ, Gong XQ, Yang HG. On the unusual properties of anatase TiO$_2$ exposed by highly reactive facets. J Phys Chem Lett 2011;2:725–34.
33. Vittadini A, Selloni A, Rotzinger FP, Gratzel M. Structure and energetics of water adsorbed at TiO$_2$ anatase 101 and 001 surfaces. Phys Rev Lett 1998;81:2954–7.
34. Kim KS, Barteau MA. Structural dependence of the selectivity of formic acid decomposition on faceted TiO$_2$ (001) surfaces. Langmuir 1990;6:1485–8.
35. Nikumbh AK, Pardeshi SK, Raste MN. A study of the thermal decomposition of copper (II) and zinc (II) malonate, maleate and succinate complexes using direct current electrical conductivity measurements. Thermochim Acta 2001;374:115–28.
36. Feist M, Kunze R, Neubert D, Witke K, Mehner H, Kemnitz E. Two oxidation states and four different coordinations of iron in an unusual chloro complex TG-MS, Raman and Mossbauer spectroscopic investigations of the thermal behaviour. Thermochim Acta 2000;361:53–60.
37. Pearson A, Bhargava SK, Bansal V. UV-switchable polyoxometalate sandwiched between TiO$_2$ and metal nanoparticles for enhanced visible and solar light photococatalysis. Langmuir. 2011;27:9245–52.
38. Liu SH, Tang WT, Chou PH. Microwave-assisted synthesis of triple 2D g-C$_3$N$_4$/Bi$_2$WO$_6$/rGO composites for ibuprofen photodegradation: kinetics, mechanism and toxicity evaluation of degradation products. Chem Eng J. 2020;387:124098.
39. Wang FL, Feng YP, Chen P, Wang YF, Su YH, Zhang QX, et al. Photocatalytic degradation of fluoroquinolone antibiotics using ordered mesoporous g-C$_3$N$_4$ under simulated sunlight irradiation: kinetics, mechanism, and antibacterial activity elimination. Appl Catal B-Environ. 2018;227:114–22.
40. Wang P, Wang J, Ming TS, Wang XF, Yu HG, Yu JG, et al. Dye-sensitization-induced visible-light reduction of graphene oxide for the enhanced TiO$_2$ photocatalytic performance. ACS Appl Mater Inter. 2013;5:2924–9.

Publisher's Note

Springer Nature remains neutral with regard to jurisdictional claims in published maps and institutional affiliations.